Macromolecules

ARTICLE

pubs.acs.org/Macromolecules

CO_2-Induced Phase Transition of Isotactic Poly-1-butene with Form III upon Heating

Lei Li, Tao Liu,* Ling Zhao,* and Wei-kang Yuan

State Key Laboratory of Chemical Engineering, East China University of Science and Technology, Shanghai 200237, P. R. China

Supporting Information

ABSTRACT: This work is aimed at studying the effect of CO_2 on the phase transition of isotactic poly-1-butene (iPB-1) with form III upon heating. The melting behaviors of form III under atmospheric N_2 and compressed CO_2 at different heating rates ranging from 1 to 20 °C/min were investigated using high-pressure differential scanning calorimetry (DSC). The results showed that the plasticization effect of CO_2 promoted melting of form III and inhibited the phase transition of form III to II as a whole. By analyzing the melting parameters obtained from the DSC measurements, we deduced that the phase transition of form III to II might comprise another transition process besides the melt-recrystallization mechanism. In-situ wide-angle X-ray diffraction (WAXD) measurement on form III under atmospheric N_2 at a heating rate of 0.25 °C/min verified that the phase transition of form III to II passed through the solid−solid phase transition before melt-recrystallization. In-situ high-pressure Fourier transform infrared (FTIR) was then used to detect the phase transition of form III under atmospheric N_2 and compressed CO_2 at the heating rate of 1 °C/min. It was also shown that the phase transition of form III to II passed through the solid−solid phase transition and melt-recrystallization under atmospheric N_2, 1 and 2 MPa CO_2. However, form II formed completely through the melt-recrystallization under 3 MPa CO_2 and could not generate with further increasing CO_2 pressure to 4 MPa. Moreover, more form I′ generated during heating through the solid−solid phase transition with increasing CO_2 pressure. Besides carbon tetrachloride solution prepared form III, the other two solutions, i.e., dilute toluene and *o*-xylene, cast form III also exhibited the similar generation processes of form II upon heating under atmospheric N_2 and compressed CO_2 as measured by in-situ high-pressure FTIR.

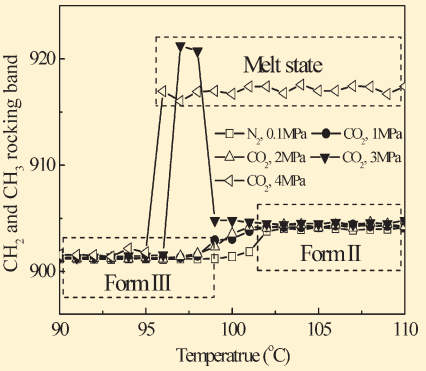

INTRODUCTION

Isotactic poly-1-butene (iPB-1), first synthesized by Natta in the 1950s,[1] is a polymorphous semicrystal polyolefin with outstanding properties, such as high creep resistance, low stiffness, good temperature, and chemical resistances.[2−5] iPB-1 may exit in four different crystal structures, designated as forms I, II, III, and I′.[6,7] Forms I and I′ have the same 3/1 helix conformation with trigonal and untwined hexagonal crystal structure, respectively.[8,9] Form II has the tetragonal unit cell packed by 11/3 helix conformation, and form III with 4/1 helix chain conformation has the orthorhombic unit cell.[10−13] The routes for preparing the iPB-1 in various crystal forms have been investigated in detail.[14,15] Crystallized from melt at atmospheric pressure, metastable form II can be obtained. However, form II is unstable under atmospheric condition and will transform into form I, a stable crystal form.[7,16−22] Forms III and I′ are usually formed by crystallization from certain dilute solutions.[23,24] Form I′ can also be obtained through crystallization from melt under high hydrostatic pressure.[25−27] In recent studies, forms I and I′ are directly crystallized from the iPB-1 melt containing different concentration of stereodefects (*rr* triads defects).[28,29]

Compressed or supercritical carbon dioxide (CO_2) is well established for using as a promising alternative to organic and other toxic or harmful solvents in polymer processing, such as polymer modification, microcellular foaming, polymer blending, particle production, and polymerization.[30−33] Dissolving CO_2 into the polymers increases the free volume of polymers and leads to an acceleration of polymer chains relaxation.[34,35] The plasticization effect depresses the glass transition temperature and melting temperature and also leads to lowering of the energy barriers making the phase transition possible at a much reduced temperarure.[36−39] The phase transitions of poly(L-lactide) (PLLA) and syndiotactic polystyrene (sPS) under CO_2 had shown significant difference from those at atmospheric conditions.[40,41] The phase transition of iPB-1 form II to I also exhibited difference from that without CO_2.[42] Whereas there are numerous investigations on CO_2-induced polymer phase transition at a constant temperature,[41,43−48] CO_2-induced polymer phase transition upon heating has been seldom studied. The phase transition of iPB-1 with form III upon heating under atmospheric condition had been wildly studied, and complicated phase transformations were involved.[49,50] It was found that form II generated during heating and form I′ could also be obtained through a solid−solid transition from form III.[51] The polymorphous transformations of form III arising during heating will provide us a good example to investigate the effect of CO_2 on the complicated phase transition upon heating.

Received: October 22, 2010
Published: May 23, 2011

In this work, the melting behaviors of iPB-1 with form III under atmospheric N_2 and compressed CO_2 at different heating rates were investigated using high-pressure differential scanning calorimetry (DSC). It was found that the phase transition of form III to II might comprise another transition process besides the melt-recrystallization mechanism. In-situ wide-angle X-ray diffraction (WAXD) measurement on form III under atmospheric N_2 at a heating rate of 0.25 °C/min verified the hypothesis. In-situ high-pressure Fourier transform infrared spectroscopy (FTIR) was then used to detect the influence of compressed CO_2 on the phase transition of form III and the effect of form III preparations on the form II generation process upon heating at a heating rate of 1 °C/min.

EXPERIMENTAL SECTION

Materials and Sample Preparations. iPB-1 pellets (PB 0110M) were kindly provided by Basell Polyolefins. Before used, they were purified by Soxhlet extraction in acetone for at least 24 h and then dried in a vacuum oven at 40 °C for 2 days. Then, they were dissolved in a 3 wt % solution of carbon tetrachloride at the solvent boiling temperature of 78 °C for 2 h. The iPB-1 film with form III was obtained by evaporating the solvent completely under atmospheric conditions. The film thickness measured by micrometer caliper was 32 ± 2 μm. CO_2 (purity: 99.9% w/w) was purchased from Air Products Co., Shanghai, China.

Wide-Angle X-ray Diffraction. WAXD of the type Rigaku D/max 2550 VB/PC X-ray diffractometer (Cu Kα Ni-filtered radiation) was used to study the modification of the prepared iPB-1 films. The scan rate was 1° (θ)/min, and the diffraction angular range was between 3° and 50° 2θ. In-situ WAXD measurement on the phase transition of form III upon heating was also performed in Rigaku D/max 2550 VB/PC X-ray diffractometer with a Paar Physica TCU 750 temperature control unit under atmospheric N_2. The operation conditions were 20 kV, 200 mA, 0.02° 2θ step^{-1} from 5° to 30°, and scanning speed 8° (θ)/min. The heating rate was controlled at 0.25 °C/min.

Differential Scanning Calorimetry. DSC (NETZSCH DSC 204 HP, Germany) was used to characterize the melting process of iPB-1 with form III under atmospheric N_2 and compressed CO_2.[52] The calorimeter was calibrated by carrying out the measurement of the melting points and the heat of fusion of In, Bi, Sn, Pb, and Zn at atmospheric N_2 and high CO_2 pressures, respectively. Under compressed CO_2 conditions, iPB-1 films were held at 30 °C for 2 h to ensure CO_2 completely diffusing into the films before heating. For each DSC measurement, about 5 ± 1 mg of the iPB-1 was heated from 30 to 150 °C at a constant heating rate. We employed several heating rates ranging from 1 to 20 °C/min.

Fourier Transform Infrared Spectroscopy. The melting process of form III was also investigated using in-situ FTIR of type Bruker Equinox-55 equipped with a Harrick high-pressure demountable liquid cell, the details of which had been described elsewhere.[53] Before being heated from 30 to 150 °C at a heating rate of 1 °C/min, the films were held at 30 °C for 2 h. FTIR spectra were recorded at a resolution of 4.0 cm^{-1} and a rate of 1 spectrum per 32 s. The IR intensities refer to the peak height. The scanned wavenumber was in the range of 4000−400 cm^{-1}.

RESULTS AND DISCUSSION

Melting Behavior of iPB-1 with Form III under Atmospheric N_2 and Compressed CO_2. The solvent and casting conditions had significant influences on the final crystal form of the obtained iPB-1 specimens.[54,55] As shown in Figure 1, the WAXD profile of the prepared iPB-1 film was the typical crystal structure of form III. It shows three strong (101), (111), and (201) reflections at 2θ = 12.2°, 17.1°, and 18.6° and two weak (200) and (120) reflections at 2θ = 14.2° and 21.3°.[56,57] Further DSC and FTIR measurements will also confirm that the iPB-1 film was in form III.

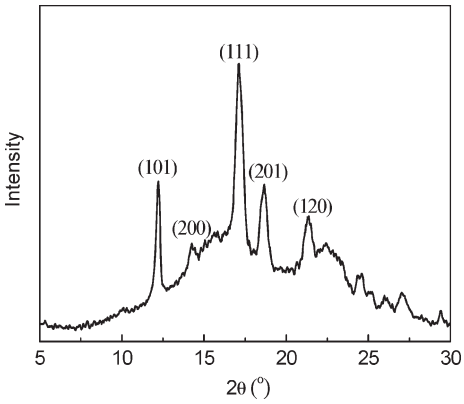

Figure 1. WAXD profile of the prepared iPB-1 film.

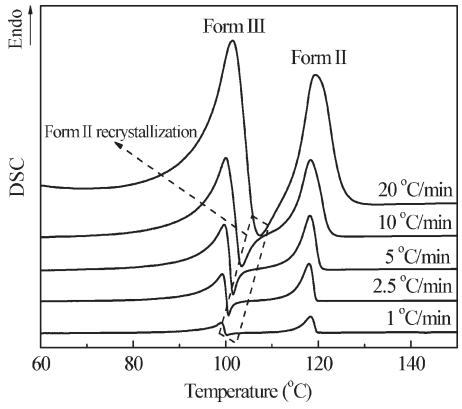

Figure 2. DSC traces of the iPB-1 with form III under atmospheric N_2 at various heating rates.

The melting behaviors of iPB-1 with form III under atmospheric N_2 at heating rates ranging from 1 to 20 °C/min, characterized by DSC, are shown in Figure 2. Two endothermic peaks were observed at all those heating rates. The first melting peak at the lower temperature was attributed to the melting of form III and the other at the higher temperature to the melting of the generated form II. Moreover, a sharp exothermic peak corresponding to recrystallization of form II was detected between the two endothermic melting peaks. With increasing heating rate, the form II recrystallization peak moves to the higher temperatures. The results were consisted with other previous work.[58,59] Lee et al. reported that the exothermic peak disappeared when the heating rate was above 20 °C/min and the endothermic peak of form II existed only as a slight shoulder at heating scan of 100 °C/min.[59] It is well-known that the DSC curves changes its shape with changing the heating rate if the phase transition is governed by the recrystallization mechanism, since the recrystallization process requires suitable time for crystallizing into another crystalline form.[60,61]

The melting behaviors of iPB-1 with form III at different CO_2 pressures ranging from 1 to 4 MPa and heating rates ranging from 1 to 20 °C/min, characterized by DSC, are shown in Figure 3. The fluctuation in the DSC curves at 2, 3, and 4 MPa was caused

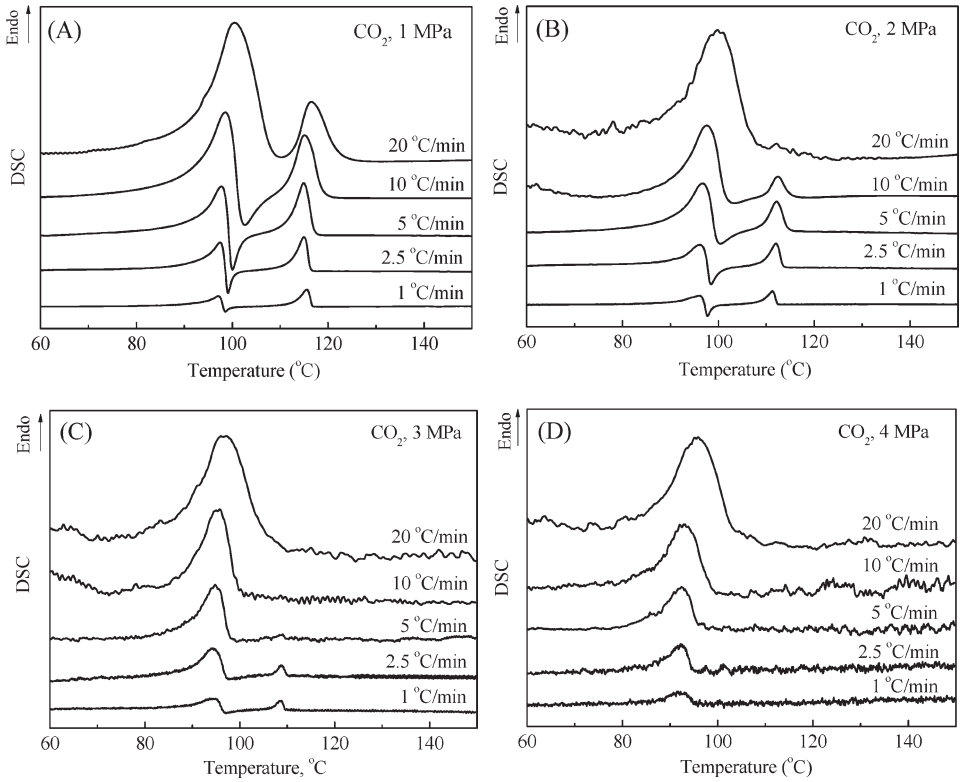

Figure 3. High-pressure DSC diagrams of the iPB-1 with form III scanned under (A) 1, (B) 2, (C) 3, and (D) 4 MPa CO_2 at various heating rates.

by the compressed CO_2. With increasing CO_2 pressure, the exothermic peak and endothermic peak of form II tended to disappear at the high heating rates. At the CO_2 pressure of 2 MPa, the exothermic peak disappeared and the endothermic peak of form II was hardly detected at the heating rate of 20 °C/min. With increasing CO_2 pressure to 3 MPa, no melting peak of form II was detected at the heating rates of 20, 10, and 5 °C/min. However, at 2 and 3 MPa, with decreasing heating rate, the exothermic peak of form II recrystallization and endothermic peak of form II melting were observed at heating rates lower than 10 and 2.5 °C/min, respectively. It indicated more time was needed for form II recrystallization upon heating at high CO_2 pressures. When melting at 4 MPa, no recrystallization and melting peaks of form II were detected even at the heating rate of 1 °C/min.

For each condition, DSC measurements were conducted at least three times, and the average melting parameters and corresponded maximum deviations were obtained. Table 1 collects the melting temperatures (T_{mIII} and T_{mII}) of forms III and II, recrystallization temperature (T_{rII}) of form II, fusion enthalpies (ΔH_{fIII} and ΔH_{fII}) of forms III and II, and recrystallization enthalpies (ΔH_{rII}) and half-recrystallization time of form II ($t_{1/2}$) of form II corresponding to the peaks and areas under the DSC curves in Figures 2 and 3. The definition of ΔH_{fIII}, ΔH_{rII}, and ΔH_{fII} is exhibited in Figure S1 of the Supporting Information. T_{mIII} increased with increasing heating rate under atmospheric N_2 and compressed CO_2, which was ascribed to increase of the superheat of form III. Moreover, as shown in Figure S2 of the Supporting Information, T_{mIII} decreased linearly with increasing CO_2 pressure at a certain heating rate with a similar value of $dT_{mIII}/dP = -1.8$ °C/MPa for various heating rates. Linear decrease of T_{mIII} as a function of CO_2 pressure was due to the plasticization effect of CO_2 on the iPB-1 and could be explained on the basis of the Flory–Huggins theory.[62,63] Another interesting observation in Table 1 was that ΔH_{fIII} decreased with decreasing heating rate under atmospheric N_2, 1, 2, and 3 MPa CO_2, which indicated less form III melted and more form III might transform into the intermediate form II without passing through melt-recrystallization with increasing relaxation time of polymer chain in form III. It was also evidenced by the gradual decrease in the melt-recrystallization rate of form II with decreasing the heating rate as demonstrated by the change of $t_{1/2}$. ΔH_{fIII} should not be the full fusion enthalpy of form III if the heating process comprised another phase transition of form III to II. However, ΔH_{fIII} did not show significant change under 4 MPa CO_2 because the form III melted completely without arranging into form II. Therefore, the full fusion enthalpy of form III could be obtained. Furthermore, ΔH_{fIII} increased with increasing CO_2 pressure at a given heating rate, indicating that dissolution of CO_2 in iPB-1 or the plasticization effect of CO_2 promoted melting of form III.

ΔH_{fII} increased with decreasing the heating rate at a certain atmosphere condition, implying that more form II had generated with increasing relaxation time of polymer chain. Meanwhile, ΔH_{fII} decreased with increasing CO_2 pressure at a given heating rate, implying that less form II had generated due to the increased plasticization effect of CO_2. $\Delta H_{rII}/\Delta H_{fII}$ characterized qualitatively the ratio of the content of form II recrystallized from melt to the total content of form II. Under atmospheric N_2 and 1 MPa CO_2, ΔH_{rII} was much lower than ΔH_{fII}, which might verify the existence of the other phase transition process of form III to II before the melt-recrystallization during heating. Meanwhile, $\Delta H_{rII}/\Delta H_{fII}$ decreased with decreasing the heating rate, indicating less form II formed through the melt-recrystallization with

Table 1. Nonisothermal Melting Parameters and Corresponding Maximum Deviations of iPB-1 with Form III at Various Heating Rates and Different Atmosphere Conditions

atmosphere	R (°C/min)	$T_{mIII} \pm 0.2$ (°C)	$\Delta H_{fIII} \pm 2.0$ (J/g)	$T_{rII} \pm 0.2$ (°C)	$\Delta H_{rII} \pm 0.5$ (J/g)	$T_{mII} \pm 0.2$ (°C)	$\Delta H_{fII} \pm 1.0$ (J/g)	$\Delta H_{rII}/\Delta H_{fII}$ (%)	$t_{1/2}$ (min)
N_2, 0.1 MPa	20	101.5	41	107.3	4.9	119.4	28	17.5	0.13
	10	100.1	39	103.5	4.8	118.3	29	16.6	0.15
	5	99.7	38	101.6	4.6	118.2	31	14.8	0.21
	2.5	99.2	37	100.6	4.2	118.2	35	12.0	0.37
	1	99.0	36	100.4	2.7	118.3	36	7.5	1.06
CO_2, 1 MPa	20	100.4	52			116.2	14		
	10	98.5	50	102.6	6.4	115.1	23	27.8	0.21
	5	97.8	49	100.1	9.2	114.9	32	28.8	0.25
	2.5	97.5	46	99.1	7.7	114.9	34	22.6	0.36
	1	97.1	44	98.6	5.1	115.5	35	14.6	0.99
CO_2, 2 MPa	20	99.8	56						
	10	97.6	54	103.3	2.0	112.4	6	33.3	0.23
	5	96.7	53	100.5	6.7	112.2	19	35.3	0.38
	2.5	96.1	52	98.5	11.2	112.0	28	40.0	0.50
	1	96.0	48	97.8	14.6	111.3	32	45.6	0.98
CO_2, 3 MPa	20	97.0	62						
	10	95.8	61						
	5	94.8	60						
	2.5	94.4	59	97.9	3.8	108.5	7	54.3	0.67
	1	94.2	57	97.0	9.1	108.5	15	60.7	1.75
CO_2, 4 MPa	20	95.9	60						
	10	92.8	61						
	5	92.5	61						
	2.5	92.3	60						
	1	91.8	61						

increasing relaxation time of polymer chain. As CO_2 pressure increased to 2 MPa, however, both ΔH_{rII} and $\Delta H_{rII}/\Delta H_{fII}$ increased with decreasing the heating rate. Especially at the low heating rates, i.e., 2.5 and 1 °C/min, ΔH_{rII} was 11.2 and 14.6 J/g, respectively, much higher than that at 1 MPa CO_2 pressure. It indicated that the plasticization effect of 2 MPa CO_2 significantly promoted the melt-recrystallization of form II and more form II generated through the melt-recrystallization with decreasing the heating rate. At CO_2 pressure of 3 MPa, ΔH_{fII} decreased to a very low level, e.g., 15 J/g even at the heating rate of 1 °C, and $\Delta H_{rII}/\Delta H_{fII}$ increased to a high level, e.g., 60.7%. It confirmed that the plasticization effect of 3 MPa CO_2 significantly inhibited the other generation process of form II before melt-crystallization and most of the form II generated through the melt-recrystallization. Meanwhile, there was a transition that ΔH_{rII} decreased in comparison with that at the CO_2 pressure of 2 MPa at the given heating rates, implying that the plasticization effect at the CO_2 pressure of 3 MPa preferred to promote melting instead of recrystallization. At the CO_2 pressure of 4 MPa, the plasticization effect of CO_2 was so strong that the iPB-1 with form III melted completely and could not recrystallize into form II even at the heating rate of 1 °C/min.

In-Situ WAXD Measurement on the Phase Transition of Form III during Heating under Atmospheric N_2. In order to verify the existence of another generation process of form II before melt-recrystallization, in-situ WAXD was applied to study the phase transition of form III upon the heating under atmospheric N_2 at a relative low heating rate of 0.25 °C/min for more form II might formed through the phase transition before melt-recrystallization as stated above. Figure 4 illustrates the variation of WAXD profiles of form III heated under atmospheric N_2 at a heating rate of 0.25 °C/min as a function of temperature. The DSC curve of form III scanned at the same heating rate under atmospheric N_2 was also exhibited at upper right corner of Figure 4. The crystal structure changes of form III during heating can be well identified by WAXD.[56] The WAXD pattern of form I′ exhibits characteristic intensity peak at $2\theta = 9.9°$ corresponding to the diffraction of crystal reflection from planes (110). Form II presents the (200) and (301) reflections at $2\theta = 11.9°$ and 18.4°. It was evident that the form III underwent a comprehensive crystal phase transition during heating. The intensities of (101) and (111) reflections at $2\theta = 12.2°$ and 17.1° of form III gradually decreased with increasing temperature. Form I′ generated at 80 °C, as demonstrated by the presence of the (110) reflection of form I′ at 9.9°, and the intensity of (110) reflection increased with increasing the temperature until to 98 °C, indicating the solid−solid phase transition of form III to I′. At 96 °C, a weak (200) reflection of form II at $2\theta = 11.9°$ was detected before form III completely melted and its intensity increased with increasing temperature, which verified the existence of another generation process of form II before from III completely melt. With the temperature further increasing, form III completely melted at 101 °C as indicated by the vanish of the (111) reflection of form III at 17.1°, which agreed well with the DSC measurement.

To have a clear insight into the phase transition of form III to II, the intensities of the (111) reflection of form III, (200) reflection of form II, and (110) reflection of form I′ as a function

dx.doi.org/10.1021/ma200988y |*Macromolecules* 2011, 44, 4836–4844

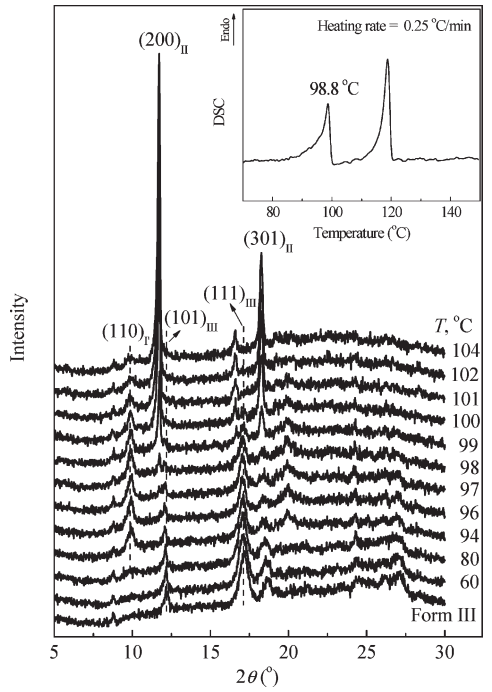

Figure 4. WAXD profiles of form III meting process under atmospheric N_2 as a function of temperature at a heating rate of 0.25 °C/min. At the upper right corner is the DSC curve of form III scanned under atmospheric N_2 at the same heating rate.

of temperature are normalized in Figure 5. It was apparent that the intensity of the (200) reflection of form II gradually increased from 96 to 99 °C and then increased abruptly at temperature above 99 °C. As shown in the DSC curve of form III in Figure 4, iPB-1 located in the endothermic peak in the temperature region of 96−99 °C and shifted to the exothermic peak at temperature above 100 °C. It demonstrated that form II generated through the melt-recrystallization since iPB-1 entered an isotropic liquid phase or mesophase at temperature above 100 °C. In the temperature region of 96−100 °C before form III completely melted, form II should formed through a solid−solid transition without entering the isotropic liquid phase or mesophase.[64] Especially at 96 and 97 °C, the majority of form III was in the solid state.

In-Situ FTIR Measurements on Phase Transition of Form III upon Heating under Atmospheric N_2 and Compressed CO_2. To further confirm the changes in the form II generation process, in-situ high-pressure FTIR was also employed to characterize the melting behavior of iPB-1 with form III under atmospheric N_2 and compressed CO_2. Because of the rapid phase transition at a fast heating rate and the relative long time during the FTIR scan period, the form III melting behavior was only studied at the heating rate of 1 °C/min. Figure 6 illustrates the FTIR spectra of iPB-1 film with form III at different temperatures. Previous work had shown there were distinct differences of form III, II, and I′ among the infrared spectrum range in 800−950 cm^{-1}. The band at 901 cm^{-1} is known to be the characteristic band of form III, while the bands at 904 and 924 cm^{-1} are corresponding to the characteristic of form II and I (or I′), respectively. They all correspond to the CH_2 and CH_3 rocking vibrations.[59,65,66]

As shown in Figure 6A, form III underwent a comprehensive crystal structure transition during heating under atmospheric N_2.

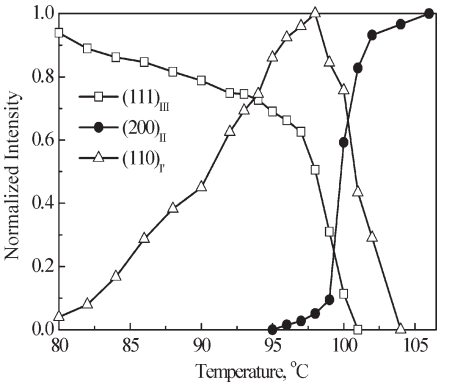

Figure 5. Normalized intensity of the (111) reflection of form III, (200) reflection of form II, and (110) reflection of form Í as a function of temperature.

The intensity of 901 cm^{-1} band decreased slightly with increasing temperature from 80 to 100 °C due to the melting of form III and solid−solid transition to form I′ as demonstrated by the appearance of a weak shoulder at 924 cm^{-1} band. Meanwhile, the intensity of 924 cm^{-1} band increased slightly with increasing the temperature, indicating the increase of form I′ content during heating. When the temperature reached 102 °C, the band at 924 cm^{-1} disappeared and the band at 901 cm^{-1} moved to 904 cm^{-1}, indicating disappearance of the forms III and I′ and generation of the form II. At this temperature, the IR spectrum gave no evidence for the appearance of the completely amorphous phase. And the band at 904 cm^{-1} kept absorbance intensity until 114 °C and vanished at 120 °C, at which a completely amorphous IR spectrum was obtained. From the DSC curve of form III melted under atmospheric N_2 at the heating rate of 1 °C/min, as shown in Figure 2, iPB-1 also melted completely at 120 °C. Jang et al.[50] had studied the form III melting process by using in-situ synchrotron small- and wide-angle X-ray scattering and found no completely amorphous pattern was recorded before form II formed. Miyoshi et al.[49] also investigated this process by using high-resolution solid-state ^{13}C NMR spectroscopy and claimed that form II phase immediately grown after melting of form III and the content of the amorphous phase continuously increased only from 47.3% at 100 °C to 59.3% at 107 °C. The in-situ FTIR measurements also revealed that the generation of form II under atmospheric N_2 comprised the solid−solid phase transition and melt-recrystallization.

The IR spectra of form III melting processes under 1 and 2 MPa CO_2, as shown in Figure 6B,C, exhibited similar phase transition behaviors in comparison with that under atmospheric N_2. The 901 cm^{-1} gradually reduced with increasing temperature. The disappearance temperatures of forms III and I′ decreased with increasing CO_2 pressure. During the generation of the form II, no completely amorphous IR spectra were detected. Amorphous IR spectra were obtained at 118 °C under 1 MPa CO_2 and at 116 °C under 2 MPa CO_2, which agreed well with the DSC results in Figure 3A,B. Meanwhile, CO_2 also promoted the generation of the form II at a lower temperature. In addition, the intensity of the 924 cm^{-1} band in IR spectra at 2 MPa was stronger than that at 1 MPa, which indicated that more form I′ generated at higher CO_2 pressure.

It should be noted that generation process of form II at 3 MPa exhibited very different from that under atmospheric N_2, 1 and 2 MPa CO_2. As shown in Figure 6D, when the temperature increased from 75 to 96 °C, the intensity of the 901 cm^{-1} band

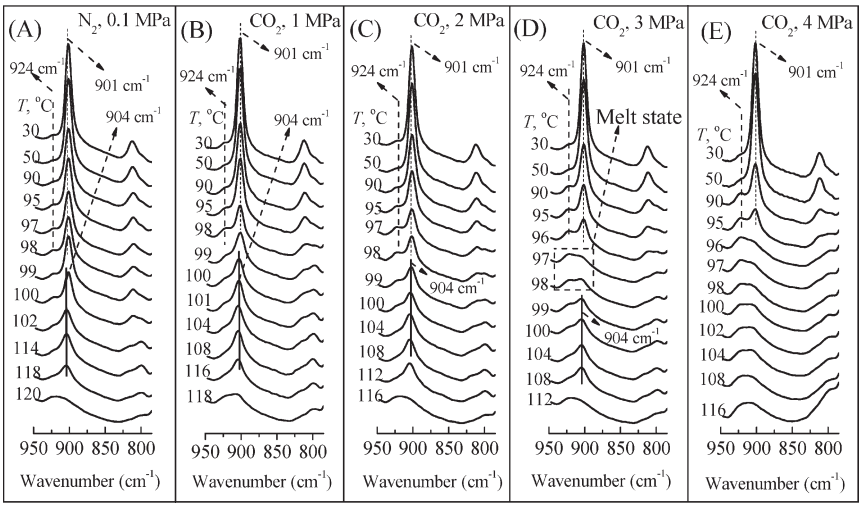

Figure 6. IR spectra of from III melting process under (A) atmospheric N_2, (B) 1 MPa CO_2, (C) 2 MPa CO_2, (D) 3 MPa CO_2, and (E) 4 MPa CO_2.

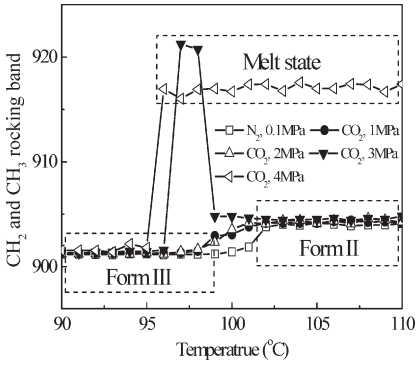

Figure 7. Change of the 901 cm^{-1} band as a function of temperature at different atmosphere conditions.

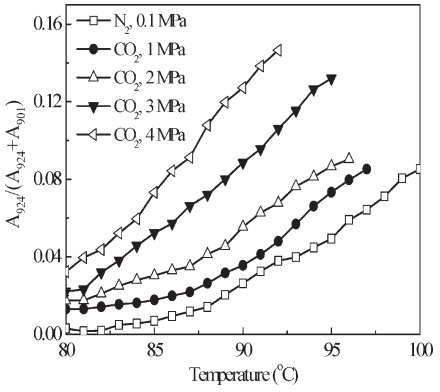

Figure 8. Dependence of form I′ relatively content on the temperature under atmospheric N_2 and compressed CO_2.

decreased slightly and that of 924 cm^{-1} band increased. However, a completely amorphous IR spectrum was obtained at 97 °C before the IR spectra of form II appeared. The band of 904 cm^{-1} began to emerge at 98 °C. The intensity of 904 cm^{-1} band increased from 100 to 104 °C, which confirmed that form II generated totally through the melt-recrystallization from form III. Moreover, the form II completely melted at 112 °C, which also corresponded to the completely melting of form II in the DSC result. Figure 6E illustrates that iPB-1 completely melted without crystallizing into form II when heated up under 4 MPa CO_2.

Figure 7 shows the spectra shifts of the 901 cm^{-1} band as a function of temperature under atmospheric N_2 and compressed CO_2. It demonstrated clearly that the coexistence of the solid−solid transition and melt-recrystallization of form III to II under atmospheric N_2, 1 and 2 MPa CO_2. When the pressure reached 3 MPa, the form II generated completely through the melt-recrystallization from the melt or mesophase. The application of high-pressure CO_2 had changed the generation process of form II. Upon further increase of the CO_2 pressure to 4 MPa, as shown in Figures 6E and 7, the forms III and I′ melted directly without recrystallizing into the form II.

The changes in the form II generation process can be explained by the plasticization effect of CO_2 on the polymer chain's motion in the amorphous phase. Handa et al.[43] had investigated the effect of compressed CO_2 on the phase transitions and polymorphism in syndiotactic polystyrene (sPS) and found sPS underwent planar mesophase to β, α to β, and γ to β transitions at different conditions of temperature and CO_2 pressure. They claimed that the extent of plasticization played an important role in determining the resulting crystal modifications. The extent of plasticization had a significant influence on the polymer chain motion and flexibility in the amorphous region.[30,34,67] The increase of polymer's chain motion influenced the polymer crystallization and phase transition behaviors. De Rosa et al. had obtained forms I and I′ directly from the melt iPB-1 prepared with metallocene catalysts. They ascribed this effect to the presence of *rr* defects in the iPB-1, which increased the flexibility of the chains and the crystallization rate of form I or I′.[28,29] The studies on the phase transition of form II to I in iPB-1 also revealed that normal stress and molecular mobility within noncrystalline regions play a crucial role in the phase transformation.[42,68−70] In the present work, the extent of CO_2 plasticization effect enhanced with increasing CO_2 pressure. The increased polymer chain motion and flexibility substantially changed the generation process of form II. This effect was also presented by the intermediate melt state at 3 MPa before recrystallization occurred. The increase in the motion and flexibility of polymer chains could make more form III melt before recrystallization. Moreover, further increased CO_2 plasticization effect, i.e., at the

dx.doi.org/10.1021/ma200988y |*Macromolecules* 2011, 44, 4836–4844

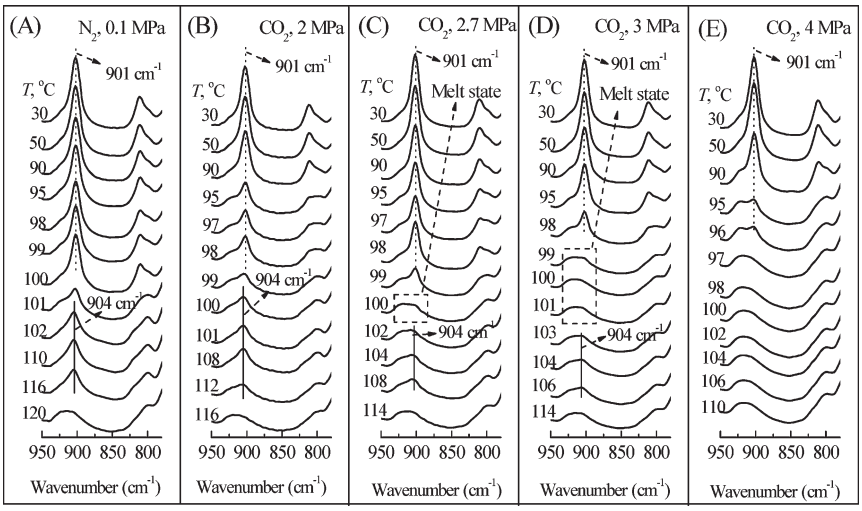

Figure 9. FTIR spectra of toluene solution prepared form III melting process under (A) atmospheric N_2, (B) 2 MPa CO_2, (C) 2.7 MPa CO_2, (D) 3 MPa CO_2, and (E) 4 MPa CO_2.

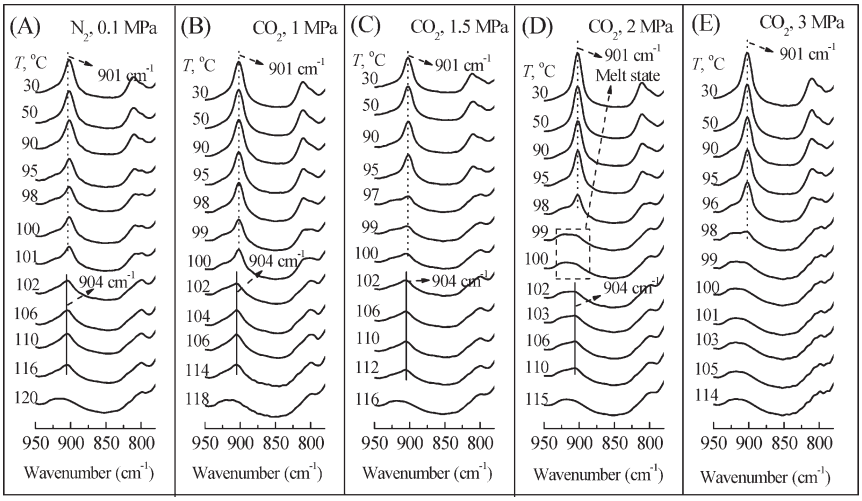

Figure 10. FTIR spectra of *o*-xylene solution prepared form III melting process under (A) atmospheric N_2, (B) 1 MPa CO_2, (C) 1.5 MPa CO_2, (D) 2 MPa CO_2, and (E) 3 MPa CO_2.

CO_2 pressure of 4 MPa, made the polymer chains motion and flexibility even more intense and polymer chains unable to reorganize into form II.

CO_2-Induced Phase Transition of Form III to I′ upon Heating. Another interesting observation from Figure 8 was that the intensity of 924 cm^{-1} band also changed with CO_2 pressure. The transformed fraction of form I′ was derived from the ratio between the absorbance band area at 924 cm^{-1} (A_{924}) and the sum of that at 901 and 924 cm^{-1} ($A_{901} + A_{924}$). The superposition of two bands was analyzed by a PEAK-FIT V4.12 program that was usually applied to deconvolute complex IR spectra. The fraction of the form I′, with respect to total fraction of crystalline phase, at various pressures as a function of temperature is shown Figure 8. It is apparent that the fraction of form I′ increased with temperature at a given pressure. The form I′ content also increased with CO_2 pressure at the same temperature. It was ascribed to the plasticization effect of CO_2, which allowed the form III to I′ transition occur at a lower temperature by increasing the polymer chain motion. That was to say more form I′ generated at a higher CO_2 pressure through elongation of the transition time.

Influence of Form III Preparations on the Phase Transition of Form III upon Heating. The DSC thermograms of dilute toluene and *o*-xylene solutions cast form III at a heating rate of 10 °C/min are shown in Figure S3 of the Supporting Information. It was apparent the solvents influenced the thermal properties of prepared form III. The form III prepared by toluene and *o*-xylene solutions has smaller ΔH_{rII} and ΔH_{fII} than that prepared by carbon tetrachloride solution.

Figure 9 illustrates the FTIR spectra of toluene solution prepared form III during heating at a heating rate of 1 °C/min under atmospheric N_2 and 2−4 MPa CO_2. As shown in Figure 9, no completely amorphous iPB-1 spectrum was detected before the 904 cm^{-1} band existed during heating, indicating the recrystallization of form II under these two conditions were not pass through the completely melt or mesophase. However, when heated under 2.7 MPa CO_2, a completely amorphous IR spectrum of iPB-1 was observed at 100 °C, as exhibited in

Figure 9C. Then, the intensity of the 904 cm^{-1} band increased with increasing the temperature until to 108 °C, which revealed the recrystallization of form II from the melt or mesophase. Completely amorphous IR spectra of iPB-1 were also detected from 99 to 101 °C during heating under 3 MPa CO_2, as shown in Figure 9D. After that, the 904 cm^{-1} band was also observed with increasing temperature. Compared with the melting process of form III under 2.7 MPa CO_2, the recrystallization of form II under 3 MPa underwent at a higher temperature and the relative intensity of form II absorbance band decreased, indicating the recrystallization of form II was gradually inhibited. Heated under 4 MPa CO_2, form III melt directly without recrystallizing into form II, as shown in Figure 9E.

Shown in Figure 10 are the FTIR spectra of *o*-xylene solution prepared form III heated under atmospheric N_2 and 1−3 MPa CO_2. For melting of the form III under atmospheric N_2 and 1−1.5 MPa CO_2, as shown in Figure 10A−C, no completely amorphous IR spectra of iPB-1 were detected before the 904 cm^{-1} band appeared, which revealed the form II was not generated totally through melt-recrystallization. Completely amorphous IR spectra of iPB-1 were detected at 99 and 100 °C before the generation of form II during heating under 2 MPa CO_2, as shown in Figure 10D, which verified that form II was recrystallized from the melt or mesophase. As shown in Figure 10E, form III directly melted under 3 MPa CO_2.

Those results above showed that the dilute toluene and *o*-xylene solutions prepared form III exhibited the similar generation processes of form II upon heating with the form III prepared by carbon tetrachloride solution under atmospheric N_2 and compressed CO_2. Moreover, high-pressure CO_2 also changed the generation process of form II into to a total melt-recrystallization.

CONCLUSION

The melting behaviors of form III under atmospheric N_2 and compressed CO_2 at different heating rates ranging from 1 to 20 °C/min were investigated using high-pressure DSC. It was shown that the plasticization effect of CO_2 promoted melting of form III and inhibited the phase transition of form III to II as a whole. By analyzing the melting parameters obtained from the DSC measurements, we deduced that the phase transition of form III to II might comprise the solid−solid transition process besides the melt-recrystallization mechanism. Under atmospheric N_2, less and less form II generated through the melt-recrystallization with decreasing the heating rate. The plasticization effect of 2 and 3 MPa CO_2 significantly promoted the melt-recrystallization of form II and more form II generated through the melt-recrystallization with decreasing the heating rate. Under 4 MPa CO_2, the plasticization effect of CO_2 was so strong that the form III was completely molten and could not recrystallize into form II, which indicated that the full fusion enthalpy of form III could be measured. In-situ WAXD measurement on form III under atmospheric N_2 at a heating rate of 0.25 °C verified that the phase transition of form III to II passed through the solid−solid phase transition before melt-recrystallization.

In-situ high-pressure FTIR was then applied to detect the phase transition of form III under atmospheric N_2 and compressed CO_2 at the heating rate of 1 °C/min. It was also shown that the phase transition of form III to II passed through the solid−solid phase transition and melt-recrystallization under atmospheric N_2, 1 and 2 MPa CO_2. However, form II generated completely through the melt-recrystallization from the melt or mesophase under 3 MPa CO_2 and could not generate with further increasing CO_2 pressure to 4 MPa. Moreover, more form I′ generated during heating through the solid−solid phase transition with increasing CO_2 pressure. Besides carbon tetrachloride solution prepared form III, the other two solutions, i.e., dilute toluene and *o*-xylene, cast form III also exhibited the similar generation processes of form II upon heating under atmospheric N_2 and compressed CO_2 as measured by in-situ high-pressure FTIR. CO_2 changed the phase transition of dilute toluene prepared form III to II to the total melt-recrystallization at 2.7 MPa, while that of dilute *o*-xylene form III to II at 2 MPa.

ASSOCIATED CONTENT

Supporting Information. Text giving experimental details on the preparation of form III from dilute toluene and *o*-xylene solutions and the definition of ΔH_{fIII}, ΔH_{rII}, and ΔH_{fII}, including figures showing definition of ΔH_{fIII}, ΔH_{rII}, and ΔH_{fII}, plots of T_{mIII} vs CO_2 pressure, and DSC curves of the different solutions prepared form III. This material is available free of charge via the Internet at http://pubs.acs.org.

AUTHOR INFORMATION

Corresponding Author

*Tel +86-21-64253175; Fax +86-21-64253528; e-mail liutao@ecust.edu.cn (T.L.), zhaoling@ecust.edu.cn (L.Z.).

ACKNOWLEDGMENT

The authors are grateful to the National Natural Science Foundation of China (Grants 20976045 and 20976046), Shanghai Shuguang Project (08SG28), Program for New Century Excellent Talents in University (NCET-09-0348), Program for Changjiang Scholars and Innovative Research Team in University (IRT0721), and the 111 Project (B08021).

REFERENCES

(1) Natta, G. *Makromol. Chem.* **1960**, *35*, 94–131.
(2) Tosaka, M.; Kamijo, T.; Tsuji, M.; Kohjiya, S.; Ogawa, T.; Isoda, S.; Kobayashi, T. *Macromolecules* **2000**, *33*, 9666–9672.
(3) Azzurri, F.; Flores, A.; Alfonso, G. C.; Calleja, F. J. B. *Macromolecules* **2002**, *35*, 9069–9073.
(4) Men, Y.; Rieger, J.; Homeyer, J. *Macromolecules* **2004**, *37*, 9481–9488.
(5) Di Lorenzo, M. L.; Righetti, M. C. *Polymer* **2008**, *49*, 1323–1331.
(6) Natta, G.; Corradini, P.; Bassi, I. *Nuovo Cimento (Suppl.)* **1960**, *15*, 52–67.
(7) Danusso, F.; Gianotti, G. *Makromol. Chem.* **1963**, *61*, 139–156.
(8) Turner-Jones, A. *J. Polym. Sci., Part B: Polym. Lett.* **1965**, *3*, 591–600.
(9) Turner-Jones, A. *Polymer* **1966**, *7*, 23–59.
(10) Turner-Jones, A. *J. Polym. Sci., Part B: Polym. Lett.* **1963**, *1*, 455–456.
(11) Cojazzi, G.; Malta, V.; Celotti, G.; Zannetti, R. *Makromol. Chem.* **1976**, *177*, 915–926.
(12) Petraccone, V.; Pirozzi, B.; Frasci, A.; Corradini, P. *Eur. Polym. J.* **1976**, *12*, 323–327.
(13) Dorset, D. L.; McCourt, M. P.; Kopp, S.; Wittmann, J. C.; Lotz, B. *Acta Crystallogr., Sect. B* **1994**, *50*, 201–208.
(14) Holland, V. F.; Miller, R. L. *J. Appl. Phys.* **1964**, *35*, 3241–3248.
(15) Luciani, L.; Seppala, J.; Lofgren, B. *Prog. Polym. Sci.* **1988**, *13*, 37–62.

(16) Boor, J.; Mitchell, J. C. *J. Polym. Sci., Part A: Gen. Pap.* **1963**, *1*, 59–84.
(17) Danusso, F.; Gianotti, G. *Makromol. Chem.* **1965**, *88*, 149–158.
(18) Powers, J.; Hoffman, J. D.; Weeks, J. J.; Quinn, F. A., Jr. *J. Res. Natl. Bur. Stand.* **1965**, *69A*, 335–345.
(19) Schaffhauser, R. J. *J. Polym. Sci., Part B: Polym. Lett.* **1967**, *5*, 839–841.
(20) Foglia, A. J. *J. Appl. Polym. Sci.: Appl. Polym. Symp.* **1969**, *11*, 1–18.
(21) Gohil, R. M.; Miles, M. J.; Petermann, J. *J. Macromol. Sci., Part B: Phys.* **1982**, *21*, 189–201.
(22) Fujiwara, Y. *Polym. Bull.* **1985**, *13*, 253–258.
(23) Miller, R. L.; Holland, V. F. *J. Polym. Sci., Part B: Polym. Lett.* **1964**, *2*, 519–521.
(24) Mathieu, C.; Stocker, W.; Thierry, A.; Wittmann, J. C.; Lotz, B. *Polymer* **2001**, *42*, 7033–7047.
(25) Armeniades, C. D.; Baer, E. *J. Macromol. Sci., Part B: Phys.* **1967**, *1*, 309–334.
(26) Nakafuku, C.; Miyaki, T. *Polymer* **1983**, *24*, 141–148.
(27) Kalay, G.; Kalay, C. R. *J. Appl. Polym. Sci.* **2003**, *88*, 814–824.
(28) De Rosa, C.; Auriemma, F.; Resconi, L. *Angew. Chem., Int. Ed.* **2009**, *48*, 9871–9874.
(29) De Rosa, C.; Auriemma, F.; Ruiz de Ballesteros, O.; Esposito, F.; Laguzza, D.; Di Girolamo, R.; Resconi, L. *Macromolecules* **2009**, *42*, 8286–8297.
(30) Kazarian, S. G.; Vincent, M. F.; Bright, F. V.; Liotta, C. L.; Eckert, C. A. *J. Am. Chem. Soc.* **1996**, *118*, 1729–1736.
(31) Nalawade, S. P.; Picchioni, F.; Janssen, L. P. B. M. *Prog. Polym. Sci.* **2006**, *31*, 19–43.
(32) Hua, C.; Chen, Z.; Xu, Q.; He, L. *J. Polym. Sci., Part B: Polym. Phys.* **2009**, *47*, 784–792.
(33) Kiran, E. *J. Supercrit. Fluids* **2009**, *47*, 466–483.
(34) Pasquali, I.; Comi, L.; Pucciarelli, F.; Bettini, R. *Int. J. Pharm.* **2008**, *356*, 76–81.
(35) Kikic, I. *J. Supercrit. Fluids* **2009**, *47*, 458–465.
(36) Chow, T. S. *Macromolecules* **1980**, *13*, 362–364.
(37) Condo, P. D.; Johnston, K. P. *Macromolecules* **1992**, *25*, 6730–6732.
(38) Asai, S.; Shimada, Y.; Tominaga, Y.; Sumita, M. *Macromolecules* **2005**, *38*, 6544–6550.
(39) Shieh, Y.-T.; Hsiao, T.-T. *J. Supercrit. Fluids* **2009**, *48*, 64–71.
(40) Ma, W.; Yu, J.; He, J. *Polymer* **2005**, *46*, 11104–11111.
(41) Marubayashi, H.; Akaishi, S.; Akasaka, S.; Asai, S.; Sumita, M. *Macromolecules* **2008**, *41*, 9192–9203.
(42) Li, L.; Liu, T.; Zhao, L.; Yuan, W. K. *Macromolecules* **2009**, *42*, 2286–2290.
(43) Handa, Y. P.; Zhang, Z.; Wong, B. *Macromolecules* **1997**, *30*, 8499–8504.
(44) Zhang, Z.; Handa, Y. P. *Macromolecules* **1997**, *30*, 8505–8507.
(45) Teramoto, G.; Oda, T.; Saito, H.; Sano, H.; Fujita, Y. *J. Polym. Sci., Part B: Polym. Phys.* **2004**, *42*, 2738–2746.
(46) Shieh, Y. T.; Hsiao, T. T.; Chang, S. K. *Polymer* **2006**, *47*, 5929–5937.
(47) Li, L.; Liu, T.; Zhao, L. *Macromol. Symp.* **2010**, *296*, 517–525.
(48) Li, L.; Liu, T.; Zhao, L.; Yuan, W. K. *Asic-Pac. J. Chem. Eng.* **2009**, *4*, 800–806.
(49) Miyoshi, T.; Hayashi, S.; Imashiro, F.; Kaito, A. *Macromolecules* **2002**, *35*, 2624–2632.
(50) Jiang, Z.; Sun, Y.; Tang, Y.; Lai, Y.; Funari, S. r. S.; Gehrke, R.; Men, Y. *J. Phys. Chem. B* **2010**, *114*, 6001–6005.
(51) Jiang, T.; Liu, M.; Fu, P.; Wang, Y.; Fang, Y.; Zhao, Q. *Polym. Eng. Sci.* **2009**, *49*, 1366–1374.
(52) Liu, T.; Hu, G. H.; Tong, G. S.; Zhao, L.; Cao, G. P.; Yuan, W. K. *Ind. Eng. Chem. Res.* **2005**, *44*, 4292–4299.
(53) Li, B.; Li, L.; Zhao, L.; Yuan, W. K. *Eur. Polym. J.* **2008**, *44*, 2619–2624.
(54) Kaszonyiova, M.; Rybnikar, F.; Geil, P. H. *J. Macromol. Sci., Part B: Phys.* **2004**, *B43*, 1095–1114.
(55) Kaszonyiova, M.; Rybnikar, K.; Geil, P. H. *J. Macromol. Sci., Part B: Phys.* **2005**, *B44*, 377–396.
(56) Nakamura, K.; Aoike, T.; Usaka, K.; Kanamoto, T. *Macromolecules* **1999**, *32*, 4975–4982.
(57) Rusa, C. C.; Wei, M.; Bullions, T. A.; Rusa, M.; Gomez, M. A.; Porbeni, F. E.; Wang, X.; Shin, I. D.; Balik, C. M.; White, J. L.; Tonelli, A. E. *Cryst. Growth Des.* **2004**, *4*, 1431–1441.
(58) Geacintov, C.; Miles, R. B.; Schuubmans, H. J. L. *J. Polym. Sci., Part C: Polym. Symp.* **1966**, *14*, 283–290.
(59) Lee, K. H.; Snively, C. M.; Givens, S.; Chase, D. B.; Rabolt, J. F. *Macromolecules* **2007**, *40*, 2590–2595.
(60) Geacintov, C.; Schotl, R. S.; Miles, R. B. *J. Polym. Sci., Part C: Polym. Symp.* **1964**, *6*, 197–207.
(61) Kawai, T.; Rahman, N.; Matsuba, G.; Nishida, K.; Kanaya, T.; Nakano, M.; Okamoto, H.; Kawada, J.; Usuki, A.; Honma, N.; Nakajima, K.; Matsuda, M. *Macromolecules* **2007**, *40*, 9463–9469.
(62) Kishimoto, Y.; Ishii, R. *Polymer* **2000**, *41*, 3483–3485.
(63) Li, B.; Zhu, X.; Hu, G.-H.; Liu, T.; Cao, G.; Zhao, L.; Yuan, W. K. *Polym. Eng. Sci.* **2008**, *48*, 1608–1614.
(64) Cheng, S. Z. D. *Phase Transitions in Polymers: The Role of Metastable States*; Elsevier Science: Amsterdam, 2008; p 24.
(65) Luongo, J. P.; Salovey, R. *J. Polym. Sci., Part A2: Polym. Phys.* **1966**, *4*, 997–1008.
(66) Goldbach, G.; Peitscher, G. *J. Polym. Sci., Part B: Polym. Lett.* **1968**, *6*, 783–788.
(67) Kazarian, S. G.; Brantley, N. H.; Eckert, C. A. *Vib. Spectrosc.* **1999**, *19*, 277–283.
(68) Goldbach, G. *Angew. Makromol. Chem.* **1973**, *29*, 213–227.
(69) Goldbach, G. *Angew. Makromol. Chem.* **1974**, *39*, 175–188.
(70) Weynant, E.; Haudin, J. M.; G'Sell, C. *J. Mater. Sci.* **1982**, *17*, 1017–1035.